Quantum-Accelerated Supercomputing Atomistic Simulations for Corrosion Inhibition

1st Karim Elgammal
Researcher at RISE Research Institute of Sweden
Stockholm, Sweden
karim.elgammal@ri.se

2nd Marc Maußner
Chief Engineer at infoteam Software AG
Bubenreuth, Germany
marc.maussner@infoteam.de

***Abstract*—This work demonstrated a proof-of-concept use case for the emerging quantum-centric supercomputing approaches combining HPC resources with quantum computers. We presented a systematic implementation of hybrid quantum-classical computational method for accelerating atomistic simulations studying corrosion inhibition. We used aluminium surface with screened inhibitor molecule on top. We combined density functional theory (DFT) with quantum algorithm through an active space embedding scheme. We chosen inhibitor molecules of 1,2,4-Triazole and 1,2,4-Triazole-3-thiol. Our implementation leveraged the ADAPT-VQE algorithm with benchmarking against classical DFT calculations, achieving binding energies of -0.386 eV and -1.279 eV for 1,2,4-Triazole and 1,2,4-Triazole-3-thiol, respectively. The binding energy of the thiol derivative aligned with experimental observations regarding sulfur-functionalized inhibitors' which could improve corrosion protection. The methodology employed the orb-d3-v2 machine learning potential for rapid geometry optimizations, followed by accurate DFT calculations using CP2K with PBE functional and Grimme's D3 dispersion corrections. CP2K is a robust DFT package that can scale on HPC classical resources of CPUs and GPUs efficiently. We also benchmarked against smaller systems and revealed that StatefulAdaptVQE implementation achieves a 5-6×computational speedup while maintaining accuracy. This work contributes to the literature studying quantum-accelerated materials science applied to periodic systems, demonstrating the viability of hybrid quantum-classical approaches for studying surface-adsorbate interactions in corrosion inhibition applications. In which, can be transferable to other applications such as carbon capture on metal oxide frameworks and solid-state battery materials studies.**

***Index Terms*—HPC, DFT, quantum simulations, quantum computing, quantum-centric supercomputing, adaptVQE, CP2K, Corrosion Inhibition, atomistic simulations, ML potentials, Qiskit**

I. Introduction

Metal surfaces in aerospace and automotive industries require effective protection against corrosion to enhance component lifespan and efficiency [1], thus it has been studied extensively both experimentally [2]–[10] and theoretically [11]–[14]. While chromium-based inhibitors historically provided robust protective capabilities [15], environmental concerns have driven a shift towards eco-friendly alternatives such as smart coatings and organic inhibitors [2], [8], [15]. These alternatives effectively form protective films on metal surfaces while maintaining compatibility with surface alloys and minimizing environmental impact [9]. Smart coating technologies have further advanced the field by enabling real-time corrosion monitoring, particularly crucial for aerospace and automotive applications [7].

Computational methods have accelerated corrosion inhibition research. High-throughput electronic structure calculations and machine learning improve the screening of potential inhibitor candidates [14]. Quantum computers, combined with classical methods [16]–[18], offer enhanced accuracy and computational efficiency. Recent advancements in quantum computing have led to the development of hybrid quantum-classical workflows that can handle periodic systems studied with DFT workflows [19]. Thus, with the growing spread of quantum hardware modalities and hardware, and already well-established HPC centers, Quantum-centric supercomputers have become a possibility, hence adding Quantum Processing Units (QPUs) as another accelerator to the existing hardware. In turn, this opened the possibility of building workflows to accelerate materials science classical simulations and port part of the calculations on the QPUs, with highly accurate and expensive theory, making sure of seamless communication between the two worlds [20]. This became possible using the quantum embedding approach [21], [22]. This approach can lead to the possibility of simulating relatively larger periodic systems with hundreds of atoms. Worth mentioning, that only a small fraction of those atoms can be computed currently on the quantum accelerator, while the remaining is done on the classical resources with classical methods.

Building on top of that, hereby, we specifically tailored a workflow for atomistic simulations of corrosion processes. Where, this work examines hybrid classical-quantum workflows for studying corrosion inhibition through simulations and quantum computer experimentation. It also provides steps and workflow to run such atomistic simulations on High Performance Computing resources (HPC) together with quantum simulations or quantum hardware. The case-study here is to model inhibitor binding to Al surfaces. And we consider it as a direct usecase that can benefit from the quantum-centric supercomputing approach.

Quantum computing have the potential to advance R&D efforts in quantum chemistry usecases. Where a hybrid quantum-classical workflow approach is crucial to perform corrosion inhibition calculations that integrate HPC systems that are widely used in running atomistic calculation codes with quan-

tum computing accelerators that can perform high-accuracy calculations through different SDKs such as Qiskit nature [23]. The framework we provide here demonstrate how quantum resources can act as accelerators for high-accuracy calculations in localized regions of large systems using quantum embedding techniques [21], enabling it to perform high-accuracy expensive methods that are at the top of Jacob's ladder [24]. Applying this workflow to corrosion inhibition usecase let the quantum embedding calculate a small fraction of the system that is responsible for the most important part of the corrosion inhibition action. Hybrid quantum-classical workflows could be key to combining utilisation of high-accuracy methods (running on the quantum part) with efficient methods (on the classical part) for advancing HPC applications in material science, balancing efficiency with accuracy [20], [25].

II. Methodology

In the following sections, we present our approach starting from the inhibitor molecules choice for the suggested workflow then workflow details followed by calculational details on both classical and quantum counterparts with overview on the quantum embedding scheme.

A. Corrosion inhibitor molecule screening

Our inhibitor screening process leveraged the CORDATA database [26], employing a multi-criteria approach to identify promising candidates for both automotive and aerospace applications. The primary screening criteria focused on efficiency, environmental stability, and structural characteristics suitable for quantum computational analysis. We targeted inhibitors demonstrating relative efficiencies above 90% in corrosion prevention compared to Cr^{6+} for AA2024 [3] and stability in the pH range of 5.5-7, which is most commonly encountered in both automotive and aerospace environments [4]. Temperature resilience requirements were specific to each industry: -30°C to 70°C for automotive applications and -50°C to 120°C for aerospace applications.

B. Candidate inhibitor molecules for our workflow

From our comprehensive screening, three candidates emerged as particularly promising, as detailed in Table I. 1,2,4-Triazole-3-thiol demonstrates broad effectiveness across both AA2024 and AA7075 alloys, with its sulfur-containing functionality showing particular affinity for copper-rich AA2024 [6]. Benzotriazole offers excellent efficiency and features an aromatic ring structure that enhances surface adhesion [3]. 2-Mercaptobenzimidazole combines both aromatic and sulfur functionalities, providing effective performance across a wide pH range [6].

We selected 1,2,4-Triazole-3-thiol as the primary candidate. This choice was motivated by several factors: its balanced molecular weight makes it suitable for quantum calculations while maintaining computational feasibility; its demonstrated effectiveness on both target alloys provides industrial relevance; and its wide pH range stability ensures practical applicability. The sulfur functionality makes it particularly effective for AA2024 alloy, due to its higher copper content [6], enabling us to study significant electronic interactions within our quantum computational framework.

The structural simplicity of 1,2,4-Triazole-3-thiol, combined with its proven inhibition efficiency, makes it an ideal candidate for developing our quantum computational methodology. Although inhibitors are typically tested on alloy structures in industrial applications, our calculations will use an Al structure with Miller indices (111) [29], [30] instead of the alloy to simplify quantum computations. This approach provides a practical balance between computational tractability and real-world applicability, a consideration particularly important for establishing proof-of-concept in quantum chemistry calculations of corrosion inhibition mechanisms.

C. Workflow overview and screening details

In our model, we simplified the problem to the form of molecule adsorption on top of a substrate. We simplified the alloy substrate to be a simple Al substrate and modelled the adsorption in vacuum. The larger the binding energy the more efficient the inhibitor molecule to attach to the surface. The screening process ideally utilizes multiple computational tools in sequence. We performed initial filtering through the CORDATA online platform using the criteria we described above, where we narrowed down our research on effective inhibitors when it comes to corrosion inhibition efficiency while being relatively small, then our calculations can converge faster, thus, will need relatively small Al substrate to model the molecule on top then we avoid the effects produced by periodic boundary conditions. Thus, we ended up choosing two inhibitors from the Triazole family where proven in experimental literature [6], [10]–[12] to be effective in corrosion inhibition due to their suitable molecular geometry, providing excellent corrosion prevention in various acidic conditions [10]. A variety of substituents on the triazole ring provide versatile inhibitory effects [10] as in 1,2,4-Triazole-3-thiol [6], [10], [12]. Fig 1 gives a comprehensive overview on the workflow steps that we are detailing in the remaining of the method section.

D. Binding energy calculational details

Adhesion properties are crucial in studying corrosion inhibition mechanisms, as they directly influence inhibitor molecule and Al surface interaction. Recent theoretical and experimental studies have established strong correlations between molecular adhesion strength and corrosion inhibition efficiency, particularly for triazole derivatives [31], [32]. González-Olvera et al. [33] demonstrated that triazole derivatives exhibiting strong surface adhesion demostrating superior corrosion protection properties. To quantify this interaction, we calculate the binding energy through this equation ($E_{\text{binding}} = E_{\text{supercell}} - E_{\text{inhibitor}} - E_{\text{substrate}}$), where stronger binding energies indicate more effective surface attachment and potentially better corrosion inhibition efficiency. This approach aligns with experimental observations by Winkler et al. [6] and

TABLE I
SELECTED CORROSION INHIBITORS AND THEIR KEY PROPERTIES

Inhibitor	Molecular Weight (g/mol)	Temperature (K)	pH Range	Efficiency (%)	Target Alloys	Ring Structure
1,2,4-Triazole [6], [10]	69.07	298	8-10	90	AA2024	Yes
1,2,4-Triazole-3-thiol [6], [10], [12]	101.13	298	4-10	70-90	AA2024, AA7075	Yes
Benzotriazole [3]	119.12	298	7-10	90-98	AA2024	Yes
2-Mercaptobenzimidazole [6]	150.2	298	4-10	90	AA2024, AA7075	Yes
(THC) [27]	227.24	303	7	91-95	AA2024	Yes
Triazine-methionine [28]	502.70	298	7	95-99	AA2024	Yes

theoretical predictions [12], where stronger molecular adhesion correlates with enhanced corrosion protection. The relationship between binding energy and inhibition efficiency has been further validated through combined theoretical and experimental studies [31].

E. Communication between classical and quantum resources

Battaglia et al. [19] have implemented an effective interface between CP2K and Qiskit nature allowing both codes to communicate messages; for implementation details refer to [34]. Figure 2 details how the communication is established and the qiskit-nature steps. The implementation leverages the socket-based communication protocol described by Battaglia et al. [19], enabling seamless integration between CP2K's classical DFT calculations and Qiskit's quantum algorithms. Figure 2 details how the communication is established and the qiskit-nature steps.

F. Computational details for the classical part

The geometry optimization step for the supercell of Al and adsorbates on top were performed using the orb-d3-v2 ML potential model [35] which can be used directly from [36]. We used CP2K code [37] for the DFT calculations and used the Perdew-Burke-Ernzerhof (PBE) [38] exchange-correlation functional within the generalized gradient approximation (GGA) [39]. We employed the Gaussian and Plane Waves (GPW) [40] method with a 500 Ry plane-wave cutoff and a relative cutoff of 60 Ry, using double-zeta valence polarized (DZVP-MOLOPT-GTH) basis sets optimized for molecular systemsZ [41]. The van der Waals interactions, crucial for accurate descriptions of inhibitor-surface interactions, were accounted for through Grimme's DFT-D3 dispersion correction scheme [42], using PBE as the reference functional. The system was treated under periodic boundary conditions with a vacuum gap of 25 Å in the z-direction to prevent interactions between periodic images and give dipole correction to the system. The surface was modeled using a 4×4 supercell of Al(111).

G. Computational details for active space embedding

Our computational approach combines classical DFT calculations with quantum computing methods through an active space embedding scheme implemented in CP2K [37] in conjunction with Qiskit nature [23], [43]. The active space was constructed with 2 active electrons in 5 orbitals around the Fermi level, where the adsorption interactions between the inhibitor and Al substrate predominantly occur. The electron repulsion integrals (ERIs) for the active space were computed using the full GPW method, maintaining periodicity in all directions. SCF convergence was set to 1.0E-6 Ha, with Broyden mixing [44] (α = 0.1, β = 1.5) employed to accelerate convergence. The embedding scheme iterations had convergency threshold of 1E-6 Ha.

The active space selection followed a systematic approach combining multiple methodologies. We employed the ActiveSpaceTransformer class as implemented in Qiskit, following the framework described by Battaglia et al. [19] for periodic systems. Meanwhile, the charge density difference (CDD) approach of Gujarati et al. [45], can be used here as well which is particularly effective for surface-adsorbate systems. This hybrid approach ensures accurate representation of both localized and periodic components of the electronic structure. A more recent implementation that could be promising for such periodic systems is described here by Weisburn et al. [46] and implemented in [47].

H. Computational details for the quantum part

Our quantum computational approach centred on the ADAPT-VQE algorithm [48], implemented through Qiskit with some proof-of-concepts executed on Braket simulators as detailed in the Appendix. The implementation follows recent developments in hybrid quantum-classical embedding methods developed by Battaglia et al. [19], particularly for periodic systems. We run our workflow with the standard VQE (we called vanilla VQE only) with the Unitary Coupled Cluster Singles and Doubles (UCCSD) ansatz [49], AdaptVQE from Qiskit with its dynamically constructed ansatz [50], [51], and StatefulVQE from qiskit-nature-cp2k [34] incorporating warm-starting techniques [22], [52]. We then expanded our benchmarking to include adaptive algorithms: AdaptVQE with gradient-based operator selection [48], Tetris-AdaptVQE following the SandboxAQ Tangelo implementation [53], and StatefulAdaptVQE with its warm-starting capabilities [19].

Our ADAPT-VQE implementation included an operator pool consisting of single and double fermionic excitations [48], with convergence criteria set to an energy threshold of 1e-6 Hartree and a gradient norm threshold of 1e-4. Classical optimization was performed using SPSA (Simultaneous Perturbation Stochastic Approximation) [54] with a maximum of 1000 iterations, a learning rate of 0.005, and a perturbation size of 0.05.

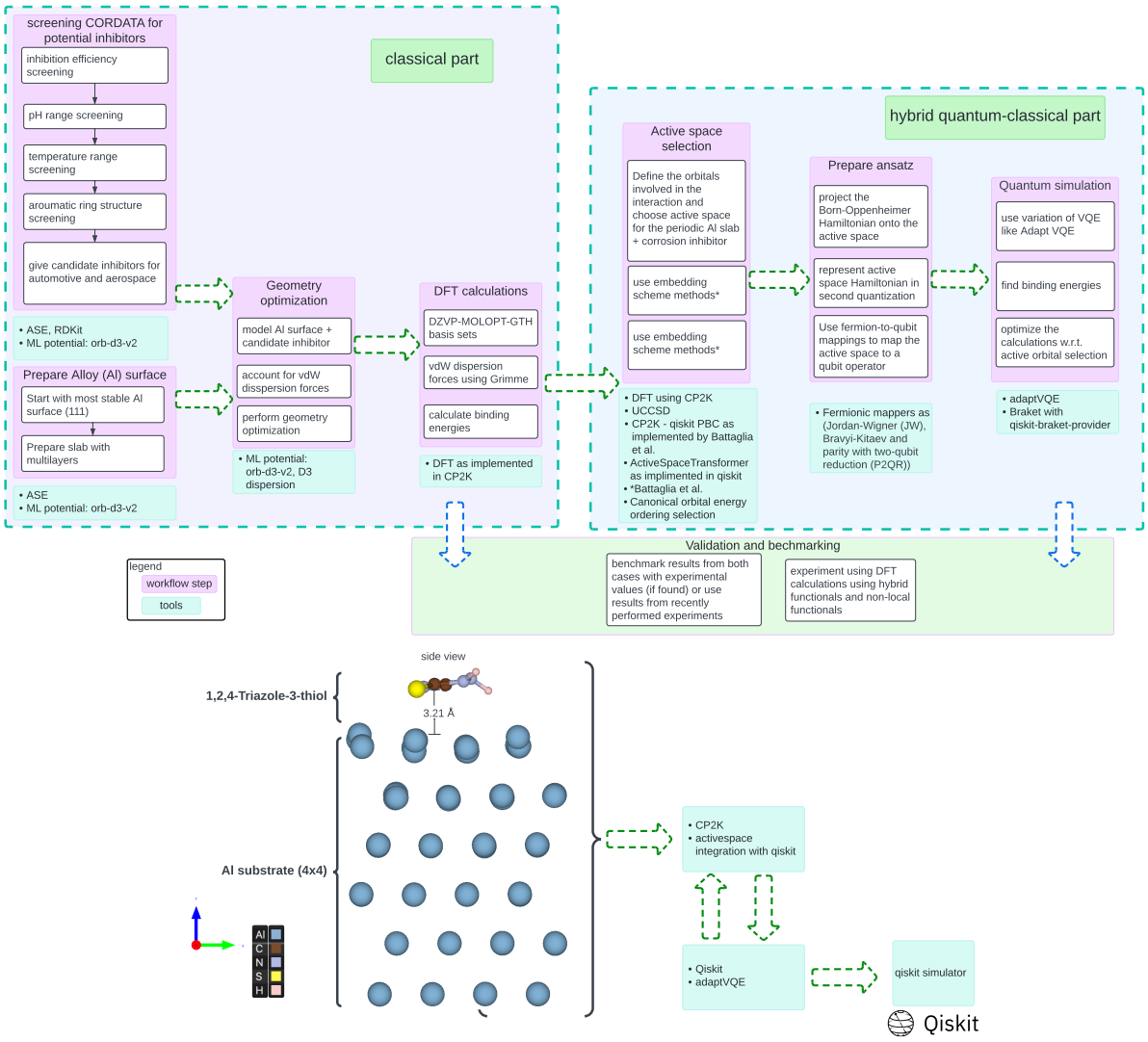

Fig. 1. The computational workflow showing the interface between classical and quantum part with the steps shown together with the tools used.

I. HPC resource utilisation

We deployed our quantum algorithms on AWS HPC EC2 instances 'hpc6a' and 'hpc7a' with 96 and 48 cores, respectively. We used CP2K docker image with MPI compilation. For initial circuit validation and algorithmic debugging, we used Qiskit's local simulator and Braket's SV1 state vector simulator, which provide high-fidelity quantum circuit simulation capabilities. We used both simulators because we encountered convergence issues with different VQE implementations. Worth mentioning that the reported results are based on Qiskit simulations on EC2 HPC instances.

III. Results

The geometry-optimized structures of 1,2,4-Triazole and 1,2,4-Triazole-3-thiol adsorbed on the 4×4 Al substrate are shown in Figs. 3. The optimization process, performed using the orb-d3-v2 ML potential model, resulted in equilibrium binding distances of 3.54Å for 1,2,4-Triazole and 3.21Å for 1,2,4-Triazole-3-thiol between the molecules and the substrate surface.

To validate our hybrid quantum-classical approach, we compared the binding energies calculated using both classical DFT and two quantum computational methods: vanilla VQE (normal VQE) and AdaptVQE, as summarized in Table III. The results show excellent agreement between classical DFT and AdaptVQE methods for both inhibitors, with AdaptVQE yielding binding energies of -0.385508 eV and -1.279064 eV for 1,2,4-Triazole and 1,2,4-Triazole-3-thiol, respectively. These values closely match the classical DFT results (-0.385512 eV and -1.279063 eV). However, the vanilla VQE implementation showed significant deviation, producing a notably higher binding energy (-2.325986 eV) for 1,2,4-Triazole.

This discrepancy between vanilla VQE and AdaptVQE results can be attributed to several factors in our computational

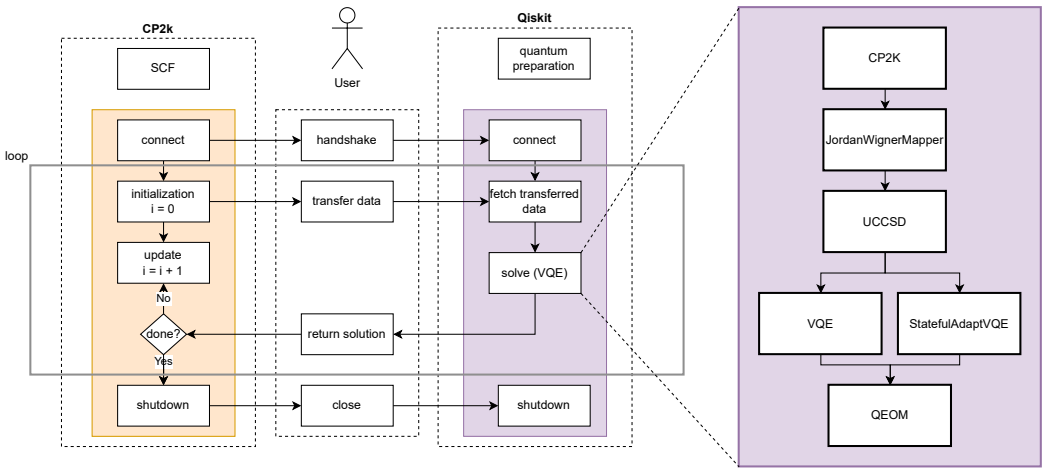

Fig. 2. The communication between CP2K and Qiskit-nature, adapted from [19].

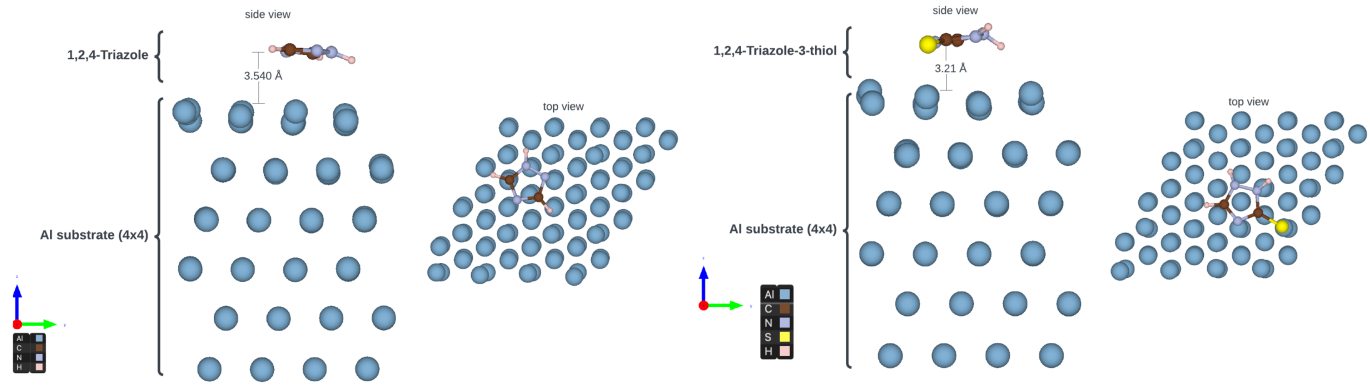

Fig. 3. Side and top of view of geometry optimised supercell of 1,2,4-Triazole (on the left) and 1,2,4-Triazole-3-thiol (on the right). Both molecules are optimised on top of Al substrate of size 4×4. The indicated binding distance was determined using the orb-d3-v2 ML potential model.

TABLE II
COMPARISON OF BINDING ENERGIES AND DISTANCES FOR DIFFERENT METHODS AND INHIBITORS

Method	Inhibitor	Binding Energy (eV)	Binding Distance (Å)
Classical DFT	1,2,4-Triazole	-0.385512	3.54
AdaptVQE	1,2,4-Triazole	-0.385508	3.54
vanilla VQE only	1,2,4-Triazole	-2.325986	3.54
Classical DFT	1,2,4-Triazole-3-thiol	-1.279063	3.21
AdaptVQE	1,2,4-Triazole-3-thiol	-1.279064	3.21

setup. First, the VQE-only case used a less stringent energy convergence threshold for the DFT embedding scheme of 2E-5. compared to the AdaptVQE implementation, using 1E-6. This difference in convergence thresholds can lead to premature convergence in the VQE case, potentially trapping the algorithm in a local minimum that yields artificially high binding energies. We have chosen to easen the convergency for VQE only case as it was very slow to converge. Additionally, the AdaptVQE implementation's adaptive operator pool selection, guided by gradient-based criteria (with gradient threshold of 1e-4), provides a more robust exploration of the quantum state space compared to the fixed ansatz structure of vanilla VQE. This advantage of AdaptVQE aligns with recent findings by Grimsley et al. [48] regarding the superiority of adaptive algorithms for electronic structure calculations.

Of particular note is the significantly stronger binding energy observed for 1,2,4-Triazole-3-thiol (-1.279 eV) compared to 1,2,4-Triazole (-0.386 eV), which can be attributed to the additional sulfur functionality enhancing the surface interaction. This observation aligns well with experimental studies by Winkler et al. [6] and Swathi et al. [12], who demonstrated that sulfur-containing triazole derivatives not only exhibit enhanced corrosion inhibition efficiency but also form more effective protective layers on metal surfaces. The stronger binding energy correlates with the shorter equilibrium binding distance (3.21Å vs 3.54Å) observed for the thiol

derivative, supporting experimental findings about sulfur's role in strengthening surface interactions and promoting more effective surface passivation [10]. This behavior is consistent with Swathi et al.'s [12] observations regarding the improved adsorption characteristics of sulfur-functionalized inhibitors on metal surfaces.

For more accurate results, we anticipate that expanding the active space to include more orbitals in the AdaptVQE calculation could lead to different binding energies compared to the classical approach. Following the active space construction approach of Battaglia et al. [19], we included 2 electrons in 5 orbitals (10 spin-orbitals in total) around the Fermi level. However, while their active space primarily captured localized defect states with one delocalized conduction band, our active space needs to describe the surface-adsorbate interaction, where both localized molecular orbitals from the inhibitor and delocalized surface states from the Al substrate contribute to the bonding [55], [56]. This interaction involves complex hybridization between molecular orbitals and substrate states [57], particularly around the Fermi level, suggesting that a larger active space might better capture these electronic coupling effects in full, once we manage to run wider active space calculation. Ofcourse considering bigger active space will be associated with more fraction of the calculation time spent on the Qiskit part, with the current setup, the Qiskit part consumed 38% of the total time while the remaining time on communication and CP2K is 62%. The computational parameters and additional technical details are provided in Table III in the Appendix.

IV. Discussion

The implementation builds upon established methodologies as implemented by Battaglia et al. in [19] while introducing flexibility to deal with adsorption-substrate models in periodic systems in quantum computing framework of Qiskit. We made some effort to use the workflow on Braket as well. Our results demonstrate that the hybrid quantum-classical approach can model corrosion inhibitor interactions, providing a new computational tool for the screening and development of environmentally-friendly corrosion inhibitors in a quantum-centric supercomputing paradigm. The strong correlation between our computed binding energies and experimental inhibition efficiencies reported in literature [10], [12] validates our computational approach and suggests its potential utility in future inhibitor design efforts. Yet, we would expect more accuracy by the quantum method if more orbitals are included in the calculations, more than the 5 orbitals used throughout the calculations due to the computational bottlenecks. We believe that our approach is a comprehensive proof-of-concept for applying quantum-centric supercomputing to modelling 2D systems in general.

Our implementation codes, input and output files are available in the attached supplementary materials to this submission and available over github through [58], the specific codes and datasets are available through [59]. For more details regarding hardware and other simulators experimentation, please refer to the relevant supplementary materials section in hardware simulation. We also provided proof-of-concept for running the applied methodology in this article to run on real hardware (superconducting, ion trap).

V. Acknowledgements

We are grateful for meetings with Airbus and BMW experts, led by Emanuele Marsili. We appreciate the Braket team in connecting with us and following up to solve challenges led by Michael Brett and Sebastian Stern as well as providing the credits on AWS Braket and EC2 HPC instances. We greatly value the technical discussions with Panagiotis Barkoutsos from IonQ in reflection of his related publications.

References

[1] B. Luan, D. Yang, X. Liu, and G.-L. Song, "15 - corrosion protection of magnesium (mg) alloys using conversion and electrophoretic coatings," pp. 541–564, 2011. [Online]. Available: https://www.sciencedirect.com/science/article/pii/B9781845697082500159

[2] R. W. Revie, *Corrosion and corrosion control: An introduction to corrosion science and engineering*. John Wiley & Sons, 2008.

[3] T. Harvey *et al.*, "The effect of inhibitor structure on the corrosion of aa2024 and aa7075," *Corrosion Science*, vol. 53, no. 6, p. 2184–2190, 2011.

[4] S. García, T. Muster, Ö. Özkanat, N. Sherman, A. Hughes, H. Terryn, J. de Wit, and J. Mol, "The influence of ph on corrosion inhibitor selection for 2024-t3 aluminium alloy assessed by high-throughput multielectrode and potentiodynamic testing," *Electrochimica Acta*, vol. 55, no. 7, pp. 2457–2465, 2010. [Online]. Available: https://www.sciencedirect.com/science/article/pii/S0013468609014984

[5] M. Laleh, M. Pathirana, and M. Y. Tan, "Site-specific local polarisation curve measurements for probing localised corrosion and inhibition," p. 111019, 2023. [Online]. Available: https://www.sciencedirect.com/science/article/pii/S0010938X23000616

[6] D. A. Winkler *et al.*, "Using high throughput experimental data and in silico models to discover alternatives to toxic chromate corrosion inhibitors," *Corrosion Science*, vol. 106, pp. 229–235, 2016.

[7] G. Zhang, L. Wu, A. Tang, Y. Ma, G.-L. Song, D. Zheng, and F. Pan, "Active corrosion protection by a smart coating based on a MgAl-layered double hydroxide on a cerium-modified plasma electrolytic oxidation coating on Mg alloy AZ31," *Corrosion Science*, vol. 139, pp. 370–382, 2018.

[8] B. E. Brycki, I. H. Kowalczyk, A. Szulc, O. Kaczerewska, and M. Pakiet, "Organic corrosion inhibitors," *IntechOpen*, 2018.

[9] J. Huang, J. Hu, J. Cai, H. Huang, J. Wei, and Q. Yu, "Inhibition effect of hydrophobic functional organic corrosion inhibitor in reinforced concrete," *Materials*, vol. 15, no. 20, p. 7124, 2022.

[10] A. Ashraf, N. Riaz, S. Muzaffar, M. Atif, and B. Bashir, "Investigating the potential of 1,2,4-triazoles as corrosion inhibitors for copper and steel: A comprehensive review," *Next Research*, vol. 1, no. 2, p. 100033, 2024. [Online]. Available: https://www.sciencedirect.com/science/article/pii/S3050475924000332

[11] A. Nahlé, R. Salim, F. El Hajjaji, M. R. Aouad, M. Messali, E. Ech-chihbi, B. Hammouti, and M. Taleb, "Novel triazole derivatives as ecological corrosion inhibitors for mild steel in 1.0 m hcl: experimental & theoretical approach," *RSC Adv.*, vol. 11, pp. 4147–4162, 2021. [Online]. Available: http://dx.doi.org/10.1039/D0RA09679B

[12] N. P. Swathi, S. Samshuddin, T. A. Aljohani, K. Rasheeda, V. D. Alva, F. Y. Alomari, and A. H. Alamri, "A new 1,2,4-triazole derivative as an excellent corrosion inhibitor: Electrochemical experiments with theoretical validation," *Materials Chemistry and Physics*, vol. 291, p. 126677, 2022. [Online]. Available: https://www.sciencedirect.com/science/article/pii/S025405842200983X

[13] F. Chiter, D. Costa, V. Maurice, and P. Marcus, "Corrosion inhibition at emergent grain boundaries studied by dft for 2-mercaptobenzothiazole on bi-crystalline copper," *npj Materials Degradation*, vol. 7, no. 1, p. 5, 2023. [Online]. Available: https://doi.org/10.1038/s41529-022-00314-5

[14] S. Li, C. Li, and F. Wang, "Computational experiments of metal corrosion studies: A review," *Materials Today Chemistry*, vol. 37, p. 101986, 2024. [Online]. Available: https://www.sciencedirect.com/science/article/pii/S2468519424000922

[15] O. Gharbi, S. Thomas, C. Smith, and N. Birbilis, "Chromate replacement: what does the future hold?" *NPJ Materials Degradation*, vol. 2, no. 1, p. 12, 2018.

[16] A. J. McCaskey, Z. P. Parks, J. Jakowski, S. V. Moore, T. D. Morris, T. S. Humble, and R. C. Pooser, "Quantum chemistry as a benchmark for near-term quantum computers," *npj Quantum Information*, vol. 5, no. 1, p. 99, 2019. [Online]. Available: https://doi.org/10.1038/s41534-019-0209-0

[17] J. Schuhmacher, G. Mazzola, F. Tacchino, O. Dmitriyeva, T. Bui, S. Huang, and I. Tavernelli, "Extending the reach of quantum computing for materials science with machine learning potentials," *AIP Advances*, vol. 12, no. 11, p. 115321, 2022.

[18] B. Camino, J. Buckeridge, P. A. Warburton, V. Kendon, and S. M. Woodley, "Quantum computing and materials science: A practical guide to applying quantum annealing to the configurational analysis of materials," *Journal of Applied Physics*, vol. 133, no. 22, p. 221102, 2023.

[19] S. Battaglia, M. Rossmannek, V. V. Rybkin, I. Tavernelli, and J. Hutter, "A general framework for active space embedding methods with applications in quantum computing," *npj Computational Materials*, vol. 10, no. 1, p. 297, 2024. [Online]. Available: https://doi.org/10.1038/s41524-024-01477-2

[20] Y. Alexeev and Others, "Quantum-centric supercomputing for materials science: A perspective on challenges and future directions," pp. 666–710, 2024. [Online]. Available: https://www.sciencedirect.com/science/article/pii/S0167739X24002012

[21] H. Ma, M. Govoni, and G. Galli, "Quantum simulations of materials on near-term quantum computers," p. 85, 2020. [Online]. Available: https://doi.org/10.1038/s41524-020-00353-z

[22] M. Rossmannek, F. Pavošević, A. Rubio, and I. Tavernelli, "Quantum embedding method for the simulation of strongly correlated systems on quantum computers," *J. Phys. Chem. Lett.*, vol. 14, no. 14, pp. 3491–3497, 2023. [Online]. Available: https://doi.org/10.1021/acs.jpclett.3c00330

[23] The Qiskit Nature developers and contributors, "Qiskit nature 0.6.0," Software package, Apr. 2023, version 0.6.0. [Online]. Available: https://doi.org/10.5281/zenodo.7828768

[24] J. P. Perdew and K. Schmidt, "Jacob's ladder of density functional approximations for the exchange-correlation energy," *AIP Conference Proceedings*, vol. 577, no. 1, pp. 1–20, 07 2001. [Online]. Available: https://doi.org/10.1063/1.1390175

[25] A. Delgado and P. Date, "Defining quantum-ready primitives for hybrid hpc-qc supercomputing: a case study in hamiltonian simulation," *Frontiers in Computer Science*, vol. 7, 2025. [Online]. Available: https://www.frontiersin.org/journals/computer-science/articles/10.3389/fcomp.2025.1528985

[26] T. L. Galvão *et al.*, "Cordata: An open data management web application to select corrosion inhibitors," *NPJ Materials Degradation*, vol. 6, no. 1, p. 48, 2022.

[27] S. Peng, G. Zhang, and X. Li, "Artificial intelligence-assisted high-throughput screening of corrosion inhibitors for aluminum alloys," *npj Materials Degradation*, vol. 8, no. 1, pp. 1–12, 2024.

[28] S. Garcia, H. Fischer, P. White, J. Mardel, Y. González-García, J. Mol, and A. Hughes, "Synthesis and anticorrosive properties of hydroxynaphthalenylmethylphosphonic compounds for aa2024," *Progress in Organic Coatings*, vol. 69, no. 2, pp. 167–174, 2010.

[29] M. Timmer and P. Kratzer, "Electron-hole spectra created by adsorption on metals from density functional theory," *Physical Review B*, vol. 79, no. 16, p. 165407, 2009.

[30] S. Kaya, P. Banerjee, S. K. Saha, B. Tüzün, and C. Kaya, "Theoretical evaluation of some benzotriazole and phospono derivatives as aluminum corrosion inhibitors: DFT and molecular dynamics simulation approaches," *RSC Advances*, vol. 6, no. 78, pp. 74 550–74 559, 2016.

[31] V. V. Mehmeti and A. R. Berisha, "Corrosion study of mild steel in aqueous sulfuric acid solution using 4-methyl-4h-1,2,4-triazole-3-thiol and 2-mercaptonicotinic acid—an experimental and theoretical study," *Frontiers in Chemistry*, vol. 5, p. 61, 2017.

[32] M. Faisal, A. Saeed, D. Shahzad, N. Abbas, F. A. Larik, P. A. Channar *et al.*, "General properties and comparison of the corrosion inhibition efficiencies of the triazole derivatives for mild steel," *Corrosion Reviews*, vol. 36, no. 6, pp. 507–545, 2018.

[33] R. González-Olvera, V. Román-Rodríguez, G. E. Negrón-Silva, A. Espinoza-Vázquez, F. J. Rodríguez-Gómez, and R. Santillán, "Multicomponent synthesis and evaluation of new 1,2,3-triazole derivatives of dihydropyrimidinones as acidic corrosion inhibitors for steel," *Molecules*, vol. 21, no. 2, p. 250, 2016.

[34] M. Rossink, "qiskit-nature-cp2k," GitHub repository, 2024, retrieved on 2024-11-02. [Online]. Available: https://github.com/mrossinek/qiskit-nature-cp2k

[35] M. Neumann, J. Gin, B. Rhodes, S. Bennett, Z. Li, H. Choubisa, A. Hussey, and J. Godwin, "Orb: A fast, scalable neural network potential," 2024. [Online]. Available: https://arxiv.org/abs/2410.22570

[36] J. DeNeutoy, B. Rhodes *et al.*, "Orb models: Fast and accurate neural network potentials with integrated D3 dispersion corrections," 2024, accessed: October 2024. [Online]. Available: https://github.com/orbital-materials/orb-models

[37] T. D. Kühne *et al.*, "CP2K: An electronic structure and molecular dynamics software package - Quickstep: Efficient and accurate electronic structure calculations," *J. Chem. Phys.*, vol. 152, no. 19, p. 194103, 2020.

[38] J. P. Perdew, K. Burke, and M. Ernzerhof, "Generalized gradient approximation made simple," *Physical Review Letters*, vol. 77, pp. 3865–3868, 1996.

[39] J. P. Perdew, J. A. Chevary, S. H. Vosko, K. A. Jackson, M. R. Pederson, D. J. Singh, and C. Fiolhais, "Atoms, molecules, solids, and surfaces: Applications of the generalized gradient approximation for exchange and correlation," *Physical Review B*, vol. 46, pp. 6671–6687, 1992.

[40] G. Lippert, J. Hutter, and M. Parrinello, "A hybrid gaussian and plane wave density functional scheme," *Molecular Physics*, vol. 92, no. 3, pp. 477–487, 1997.

[41] J. VandeVondele and J. Hutter, "Gaussian basis sets for accurate calculations on molecular systems in gas and condensed phases," *The Journal of Chemical Physics*, vol. 127, no. 11, p. 114105, 2007.

[42] S. Grimme, J. Antony, S. Ehrlich, and H. Krieg, "A consistent and accurate ab initio parametrization of density functional dispersion correction (dft-d) for the 94 elements h-pu," *The Journal of Chemical Physics*, vol. 132, no. 15, p. 154104, 2010.

[43] Qiskit contributors, "Qiskit: An open-source framework for quantum computing," 2023.

[44] D. D. Johnson, "Modified broyden's method for accelerating convergence in self-consistent calculations," *Physical Review B*, vol. 38, pp. 12 807–12 813, 1988.

[45] T. P. Gujarati, M. Motta, T. N. Friedhoff, J. E. Rice, N. Nguyen, P. K. Barkoutsos, R. J. Thompson, T. Smith, M. Kagele, M. Brei, B. A. Jones, and K. Williams, "Quantum computation of reactions on surfaces using local embedding," *npj Quantum Information*, vol. 9, no. 1, p. 88, 2023.

[46] L. P. Weisburn, M. Cho, M. Bensberg, O. R. Meitei, M. Reiher, and T. V. Voorhis, "Multiscale embedding for quantum computing," 2024. [Online]. Available: https://arxiv.org/abs/2409.06813

[47] "Bootstrap embedding (be) method for quantum embedding," https://github.com/oimeitei/quemb?tab=readme-ov-file, 2024, accessed: 2024-12-03.

[48] O. Higgott, D. Wang, and S. Brierley, "Variational Quantum Computation of Excited States," *Quantum*, vol. 3, p. 156, Jul. 2019. [Online]. Available: https://doi.org/10.22331/q-2019-07-01-156

[49] J. Romero, R. Babbush, J. R. McClean, C. Hempel, P. J. Love, and A. Aspuru-Guzik, "Strategies for quantum computing molecular energies using the unitary coupled cluster ansatz," *Quantum Science and Technology*, vol. 4, no. 1, p. 014008, 2018.

[50] H. L. Tang, V. Shkolnikov, G. S. Barron, H. R. Grimsley, N. J. Mayhall, E. Barnes, and S. E. Economou, "Qubit-adapt-vqe: An adaptive algorithm for constructing hardware-efficient ansätze on a quantum processor," *PRX Quantum*, vol. 2, p. 020310, Apr 2021. [Online]. Available: https://link.aps.org/doi/10.1103/PRXQuantum.2.020310

[51] K. Dalton, C. K. Long, Y. S. Yordanov, C. G. Smith, C. H. W. Barnes, N. Mertig, and D. R. M. Arvidsson-Shukur, "Quantifying the effect of gate errors on variational quantum eigensolvers for quantum chemistry," *npj Quantum Information*, vol. 10, no. 1, Jan. 2024. [Online]. Available: http://dx.doi.org/10.1038/s41534-024-00808-x

[52] M. Rossmannek, P. K. Barkoutsos, P. J. Ollitrault, and I. Tavernelli, "Quantum HF/DFT-embedding algorithms for electronic structure calculations: Scaling up to complex molecular systems," *The Journal of Chemical Physics*, vol. 154, no. 11, p. 114105, 2021.

[53] P. G. Anastasiou, Y. Chen, N. J. Mayhall, E. Barnes, and S. E. Economou, "Tetris-adapt-vqe: An adaptive algorithm that yields shallower, denser circuit ansätze," *Physical Review Research*, vol. 6,

no. 1, Mar. 2024. [Online]. Available: http://dx.doi.org/10.1103/PhysRevResearch.6.013254
[54] J. C. Spall, "Multivariate stochastic approximation using a simultaneous perturbation gradient approximation," *IEEE transactions on automatic control*, vol. 37, no. 3, pp. 332–341, 1992.
[55] T. Kumagai, F. Hanke, S. Gawinkowski, J. Sharp, K. Kotsis, J. Waluk, M. Persson, and L. Grill, "Controlling intramolecular hydrogen transfer in a porphycene molecule with single atoms or molecules located nearby," *Nature Chemistry*, vol. 6, pp. 41–46, 2013.
[56] Z. Cheng, S. Du, W. Guo, L. Gao, Z. Deng, N. Jiang, H. Guo, H. Tang, and H. Gao, "Direct imaging of molecular orbitals of metal phthalocyanines on metal surfaces with an o2-functionalized tip of a scanning tunneling microscope," *Nano Research*, vol. 4, pp. 523–530, 2011.
[57] F. Hanke, S. Haq, R. Raval, and M. Persson, "Heat-to-connect: surface commensurability directs organometallic one-dimensional self-assembly," *Acs Nano*, vol. 5, pp. 9093–9103, 2011.
[58] K. Elgammal and M. Maußner, "inhibitq project repository," https://github.com/MarcMaussner/2024_inhibitQ/, 2024.
[59] ——, "Quantum-accelerated supercomputing atomistic simulations for corrosion inhibition," 2024. [Online]. Available: https://archive.materialscloud.org/record/2024.211
[60] ASE contributors, "The atomic simulation environment—a python library for working with atoms," *Journal of Physics: Condensed Matter*, vol. 29, no. 27, p. 273002, 2017. [Online]. Available: http://stacks.iop.org/0953-8984/29/i=27/a=273002
[61] E. R. Sayfutyarova, Q. Sun, G. K.-L. Chan, and G. Knizia, "Automated construction of molecular active spaces from atomic valence orbitals," *Journal of Chemical Theory and Computation*, vol. 13, no. 9, pp. 4063–4078, 2017. [Online]. Available: https://doi.org/10.1021/acs.jctc.7b00128
[62] S. Bravyi, J. M. Gambetta, A. Mezzacapo, and K. Temme, "Tapering off qubits to simulate fermionic hamiltonians," *arXiv preprint arXiv:1701.08213*, 2017.
[63] Qiskit Community, "Qiskit aer," GitHub repository, 2024, retrieved on 2024-11-03. [Online]. Available: https://github.com/Qiskit/qiskit-aer
[64] B. Nachman, M. Urbanek, W. A. de Jong, and C. W. Bauer, "Unfolding quantum computer readout noise," *npj Quantum Information*, vol. 6, no. 1, pp. 1–7, 2020.
[65] Qiskit Community, "Configure error-mitigation," Online documentation, 2024, retrieved on 2024-11-03. [Online]. Available: https://docs.quantum.ibm.com/guides/configure-error-mitigation
[66] K. Temme, S. Bravyi, and J. M. Gambetta, "Error mitigation for short-depth quantum circuits," *Physical Review Letters*, vol. 119, no. 18, p. 180509, 2017.
[67] R. LaRose, A. Mari, P. J. Karalekas, N. Shammah, K. Heya, and C. A. Morrison, "Mitiq: A software package for error mitigation on noisy quantum computers," *Quantum*, vol. 6, p. 774, 2022.
[68] A. Kandala, K. Temme, A. D. Córcoles, A. Mezzacapo, J. M. Chow, and J. M. Gambetta, "Error mitigation extends the computational reach of a noisy quantum processor," *Nature*, vol. 567, no. 7749, pp. 491–495, 2019.
[69] CP2K Developers, "Cp2k input reference - active space," Online Manual, 2024, retrieved on 2024-03-11. [Online]. Available: https://manual.cp2k.org/trunk/CP2K_INPUT/FORCE_EVAL/DFT/ACTIVE_SPACE.html
[70] Amazon Web Services, "Amazon braket: A fully managed quantum computing service," *AWS Documentation*, 2024. [Online]. Available: https://docs.aws.amazon.com/braket/
[71] ——, "Amazon braket sdk," GitHub repository, 2024, retrieved on 2024-11-01. [Online]. Available: https://github.com/amazon-braket/amazon-braket-sdk-python
[72] Qiskit Community, "qiskit-braket-provider," GitHub repository, 2024, retrieved on 2024-11-02. [Online]. Available: https://github.com/qiskit-community/qiskit-braket-provider
[73] K. Elgammal, "qiskit-nature-cp2k-updated," GitHub repository, 2024, retrieved on 2024-11-02. [Online]. Available: https://github.com/KarimElgammal/qiskit-nature-cp2k/tree/fix-qiskit1.x-compatibility
[74] Amazon Web Services, *High performance computing (HPC) instances*, Amazon Web Services, 2024, amazon EC2 HPC Instances. [Online]. Available: https://docs.aws.amazon.com/ec2/latest/instancetypes/hpc.html
[75] J. M. A. Hualde, M. Kowalik, L. Remme, F. E. Wolff, J. van Velzen, R. Bottcher, C. Weimer, J. Krauser, and E. Marsili, "Quantum computing in corrosion modeling: Bridging research and industry," 2024. [Online]. Available: https://arxiv.org/abs/2412.07933

APPENDIX

A. Computational methods and parameters

Table III provides a detailed computational parameters and methods used in this work including the proof-of-concept calculations we detailing here in the appendix. The parameters were chosen to balance computational efficiency with accuracy, particularly for the hybrid quantum-classical calculations of surface-adsorbate systems, such as the corrosion inhibitor example here. Our classical computational approach involved a two-step process of classical calculations then a hybrid quantum-classical approach: geometry optimizations were conducted using the Atomic Simulation Environment (ASE) [60] with orb-d3-v2 ML potential model [35], [36], which integrates Grimme's D3 dispersion corrections directly into their NN potential. Dispersion forces play a crucial role in this system and the orb models have native support for periodic systems making them especially suitable for our surface calculations. Our shortlisted inhibitors contain aromatic rings for π-π stacking interactions and demonstrate strong electron transfer potential with Al [30], that was based on the criteria we discussed in choosing inhibitors. We have chosen a substrate of 4×4 to avoid the interactions between repeated cells in the xy directions between the images of the inhibitor molecule.

B. Quantum algorithm benchmarking

We conducted systematic benchmarking of various VQE implementations to validate our computational approach and establish optimal parameters for the surface-adsorbate calculations. We benchmarked various algorithms of calculating the ground state energies using simpler systems using the LiH molecule. The benchmarking process consisted of three main components:

1) Standard VQE algorithm comparison: Initial benchmarking compared three VQE implementations using LiH as a test system. Results showed that AdaptVQE demonstrated superior performance, reducing computational time by approximately 50% while maintaining comparable accuracy (Table IV). This efficiency gain aligns with recent findings by Grimsley et al. [48] on the advantages of adaptive algorithms for electronic structure calculations.

2) Adaptive VQE variant analysis: Further comparison of different adaptive VQE implementations revealed that StatefulAdaptVQE exhibited exceptional performance, achieving a 5-6×speedup through its implementation of warm-starting techniques [52] (Table V). The TetrisAdaptVQE implementation showed limited improvement opportunities, with only 12×the tetris feature applied in our test case.

Error mitigation assessment: To evaluate quantum hardware implementation challenges, we conducted benchmarking studies using H_2 as a test system across different execution environments for AdaptVQE implementation in Qiskit (Table VI). Our error mitigation strategy incorporated both readout error mitigation techniques [64] and zero-noise extrapolation (ZNE) [66], [68], implemented through the Mitiq package [67]. The comparison between ideal simulation, noisy simulation using FakeVigo device, and FakeVigo with ZNE revealed substantial variations in ground state energies, from -1.1373 Ha in ideal conditions to 0.4083 Ha under noise. The application of ZNE significantly improved accuracy by recovering a ground state energy of -1.0305 Ha, demonstrating the crucial importance of error mitigation strategies in quantum hardware implementations. These results align with recent findings by Kandala et al. [68] and Temme et al. [66], and we further validated them through additional tests using local noisy simulators.

C. Active space analysis

Our active space selection methodology combined the ActiveSpaceTransformer implementation from Qiskit with the embedding approach as implemented in CP2K code [37] as detailed in their manual [69], utilizing the HARTREE-FOCK model to calculate active space interaction Hamiltonian. Following the recent framework by Battaglia et al. [19], we employed the CANONICAL method for orbital selection, which orders orbitals based on their energy. This approach proved particularly effective for our surface-adsorbate systems, as the energy-ordered canonical orbitals naturally aligned with the orbitals around the Fermi level that are crucial for the adsorption process. The analysis revealed several significant electronic contributions to the corrosion inhibition mechanism, including the π-system of the triazole ring, the lone pair electrons on the sulfur atom (specifically for 1,2,4-Triazole-3-thiol), and the surface states at the Al(111) interface. These electronic features and their interactions align well with experimental observations by Winkler et al. [6] and Swathi et al. [12] regarding the mechanism of corrosion inhibition by triazole derivatives, validating our computational approach to active space selection.

D. The used Hamiltonian

The electronic Hamiltonian was constructed following the second-quantized formalism [52]:

$$\hat{H} = \sum_{pq} h_{pq} \hat{a}_p^\dagger \hat{a} q + \frac{1}{2} \sum pqrs g_{pqrs} \hat{a}_p^\dagger \hat{a}_r^\dagger \hat{a} s \hat{a} q \qquad (1)$$

where hpq and $gpqrs$ represent the one- and two-electron integrals computed within the active space. The fermionic operators were mapped to qubit operators using the parity mapping with two-qubit reduction [62], which was chosen for its efficient handling of particle number conservation.

E. Simulation SDKs and hardware

We made some effort in running our simulations on Braket SDK [70], [71] through the integration tool qiskit-braket-provider [72]. We had to upgrade it to be compatible with latest qiskit version 1.x for our special case of simulations as in [73]. Though at the time of writing, simulations of this chemistry hybrid use case with braket local simulation SV1, IonQ Aria and IQM Garnet are still challenging for us, that is why our results presented in the results section focused

TABLE III
SUMMARY OF COMPUTATIONAL METHODS AND PARAMETERS

Method/Component	Details
Classical Calculations	
Geometry Optimization	ASE [60] with orb-d3-v2 model [36]
Dispersion Corrections	Grimme's D3 (integrated into neural network potential)
Surface Model	Al(111) 4×4 supercell
DFT Calculations	
Functional	PBE [38] with GGA implementation [39]
Basis Set	DZVP-MOLOPT-GTH (double-zeta valence polarized)
Method	GPW [40], plane-wave cutoff: 500 Ry, relative cutoff: 60 Ry
van der Waals	DFT-D3 [42] with PBE reference functional
Vacuum Gap	40 Å (z-direction)
Electronic Temperature	1000 K (Fermi-Dirac distribution)
SCF Convergence	1.0E-6 Ha, Broyden mixing (α = 0.1, β = 1.5)
Active Space Parameters	
Configuration	2e, 5o (2 active electrons in 5 orbitals)
Selection Method	ActiveSpaceTransformer (Qiskit implementation), canonical orbital energy ordering selection [61]
Quantum Calculations	
Primary Algorithm	ADAPT-VQE [48] from Qiskit, StatefulAdaptVQE from qiskit-nature-cp2k [34]
Qubit Mapping	Parity with two-qubit reduction [62]
Convergence Criteria	Energy threshold: 1e-6 Hartree, gradient norm: 1e-4
Classical Optimizer	SPSA [54] (learning rate: 0.005, perturbation size: 0.05, max iterations: 1000)
Quantum Hardware & Simulation	
Simulators	Qiskit local and Aer [63], Braket local and SV1
Hardware	IonQ Aria (via AWS Braket), IQM Garnet
Error Mitigation	Readout error mitigation [64] via Qiskit Runtime [65], Zero-noise extrapolation [66] via Mitiq [67]

TABLE IV
COMPARISON OF VQE ALGORITHM PERFORMANCE

Algorithm	Runtime (s)	Ground State Energy (Ha)
VQE	3654	-7.8824
StatefulVQE	3134	-7.8824
AdaptVQE	1552	-7.8820

TABLE V
PERFORMANCE OF ADAPTIVE VQE VARIANTS

Algorithm	Runtime (s)	Ground State Energy (Ha)
AdaptVQE	1258	-7.8820
StatefulAdaptVQE	272	-7.8802
TetrisAdaptVQE	1493	-7.8820

on qiskit local simulations on HPC EC2 instances (Hpc6a, Hpc7a) [74].

For actual quantum computations, we used IonQ's Aria quantum processor and IQM's Garnet quantum processor, accessed through the AWS Braket platform [70]. We managed to use it only for the benchmarking phase on small systems and not yet on our calculational cells.

TABLE VI
IMPACT OF ERROR MITIGATION ON GROUND STATE ENERGY CALCULATIONS

Environment	Ground State Energy (Ha)
Ideal Simulation	-1.1373
FakeVigo (Noisy)	0.4083
FakeVigo + ZNE	-1.0305

TABLE VII
BENCHMARKING RUNTIME OF QEOM/VQE OF H_2

Environment	Runtime (s)
qEOM qiskit local	6.42
qEOM braket local	319.13
qEOM braket SV1	981.43
qEOM braket SV1 via HybridJob	1255.07
VQE braket local	10.03
VQE braket SV1	931.74
VQE braket SV1 via HybridJob	833.83

F. Benchmarking runtime of Qiskit and Braket

To find the most efficient way to update our workflow, we did some benchmarking of the runtime needed to calculate qEOM and VQE of H_2 for different setups. We measured the runtime when calculating qEOM with qiskit natively with local esitmator. After that we used the qiskit-native-provider to bridge to braket and measured runtime for BraketLocal (on local machine), SV1 (on-demand simulation) and SV1 in a HybridJob (fully managed orchestration of hybrid quantum-classical algorithms with priority queueing for quantum tasks and automatic resource management). The last series of measurements was done for calculation of VQE of H_2 natively in braket for BraketLocal, SV1 and SV1 in a HybridJob. The results are shown in VII. So we need to improve the performance by reducing the communication time, when using real devices provided from AWS. Worthmentioning, a recent benchmark for resource estimation can be found here [75] for corrosion inhibition across different simulation scales.